High Order Finite Difference and Finite Volume WENO Schemes and Discontinuous Galerkin Methods for CFD

Chi-Wang Shu[1]

Division of Applied Mathematics

Brown University

Providence, Rhode Island 02912

ABSTRACT

In recent years high order numerical methods have been widely used in computational fluid dynamics (CFD), to effectively resolve complex flow features using meshes which are reasonable for today's computers. In this paper we review and compare three types of high order methods being used in CFD, namely the weighted essentially non-oscillatory (WENO) finite difference methods, the WENO finite volume methods, and the discontinuous Galerkin (DG) finite element methods. We summarize the main features of these methods, from a practical user's point of view, indicate their applicability and relative strength, and show a few selected numerical examples to demonstrate their performance on illustrative model CFD problems.

Key Words: Weighted essentially non-oscillatory, discontinuous Galerkin, finite difference method, finite volume method, computational fluid dynamics.

[1]E-mail: shu@cfm.brown.edu. Research supported by ARO grants DAAG55-97-1-0318 and DAAD19-00-1-0405, NSF grants DMS-9804985 and ECS-9906606, NASA Langley grant NAG-1-2070 and Contract NAS1-97046 while the author was in residence at ICASE, NASA Langley Research Center, Hampton, VA 23681-2199, and AFOSR grant F49620-99-1-0077.

1 Introduction

In recent years high order numerical methods have been widely used in computational fluid dynamics (CFD), to effectively resolve complex flow features. In this paper we refer to high order methods by those with order of accuracy at least three. Traditionally, first and second order numerical methods are often preferred in practical calculations, because of their simplicity and robustness (i.e. one can always get some output, although it may not be very accurate). On the other hand, high order methods often give the impression of being complicated to understand and to code, and costly to run (on the same mesh compared with lower order methods), and less robust (the code may blow up in tough situations when the lower order methods still give stable output). In this paper, we hope to at least partially disapprove this impression about high order methods, using three typical types of high order methods as examples.

Before we move on to the details of high order methods, let us point out that, at least in certain situations, the solution structures are so complicated and the time of evolution of these structures so long that it is impractical to use low order methods to obtain an acceptable resolution. Often such problems involve both shocks and complicated smooth region structures, calling for special non-oscillatory type high order schemes which are emphasized in this paper. A very simple example to illustrate this is the evolution of a two dimensional periodic vortex for the compressible Euler equations, which was first used in [41]. One could put a shock to this problem so that it becomes a problem of shock interaction with vortex, which is very typical in aeroacoustics. However we will consider the solution without a shock here as it admits an analytically given exact solution, making it easier to compare numerical resolutions of different schemes. The Euler equations are given by a conservation law

$$u_t + f(u)_x + g(u)_y = 0, \tag{1.1}$$

where

$$u = (\rho, \rho u_1, \rho u_2, E),$$

$$f(u) = (\rho u_1, \rho u_1^2 + p, \rho u_1 u_2, u_1(E+p)), \qquad g(u) = (\rho u_2, \rho u_1 u_2, \rho u_2^2 + p, u_2(E+p)),$$

Here ρ is the density, (u_1, u_2) is the velocity, E is the total energy, p is the pressure, related to the total energy E by

$$E = \frac{p}{\gamma - 1} + \frac{1}{2}\rho(u_1^2 + u_2^2)$$

with $\gamma = 1.4$ for air. The periodic vortex problem is set up in a computational domain [0,10]×[0,10]. The boundary condition is periodic in both directions. The initial condition is given by

$$(u_1(x, y, 0), u_2(x, y, 0)) = (1, 1) + \frac{\epsilon}{2\pi} e^{0.5(1-r^2)}(-\overline{y}, \overline{x}),$$

$$T(x, y, 0) = 1 - \frac{(\gamma - 1)\epsilon^2}{8\gamma\pi^2} e^{1-r^2}, \qquad S(x, y, 0) = 1,$$

where the temperature T and the entropy S are related to the density ρ and the pressure p by

$$T = \frac{p}{\rho}, \qquad S = \frac{p}{\rho^\gamma},$$

and $(\overline{x}, \overline{y}) = (x - 5, y - 5)$, $r^2 = \overline{x}^2 + \overline{y}^2$, and the vortex strength $\epsilon = 5$.

It can be readily verified that the Euler equations with the above initial conditions admit an exact solution which is convected with the speed $(1, 1)$ in the diagonal direction. Because of the periodic boundary condition, we can simulate this flow for a very long time. We first show the simulation results at $t = 10$, namely after one time period. When we perform the simulation of a second order finite difference MUSCL type TVD scheme and a fifth order finite difference WENO scheme with the *same* uniform mesh of 80^2 points, for this relatively short time, although the second order scheme gives inferior results comparing with that of the fifth order scheme, Fig. 1.1, it may be argued that the second order scheme still gives an acceptable resolution. If we increase the number of mesh points for the second order scheme to 200^2 points, see Fig. 1.3, left, then the resolution is roughly comparable to that of the fifth order WENO scheme using 80^2 points in Fig. 1.1, right. A two dimensional time dependent simulation with a 200^2 mesh has $2.5^3 = 15.6$ times more space time mesh points than a 80^2 mesh. Considering that the CPU time of a fifth order finite difference WENO scheme

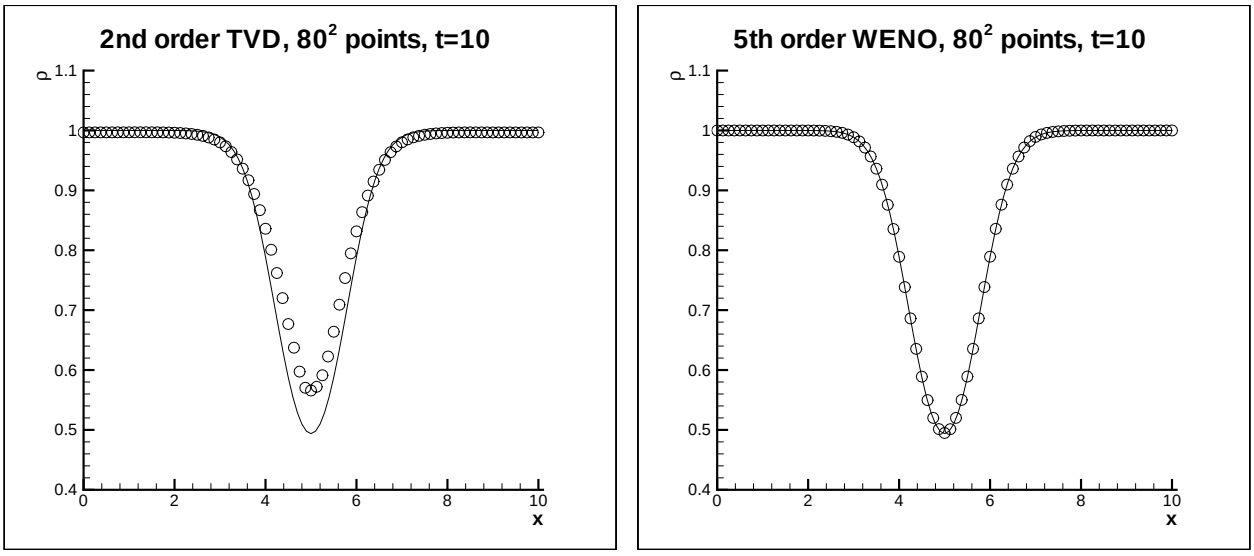

Figure 1.1: Vortex evolution. Cut at $x = 5$. Density ρ. 80^2 uniform mesh. $t = 10$ (after one time period). Solid: exact solution; circles: computed solution. Left: second order TVD scheme; right: fifth order WENO scheme.

is roughly 3 to 8 times more than that of a second order TVD scheme on the same mesh (depending on the specific forms of the schemes and time discretization), we could conclude that the second order TVD scheme has a larger but still comparable CPU cost than the fifth order WENO scheme to reach the same resolution, for this problem with relatively short time. When we look at the result at $t = 100$, namely after ten time periods, the situation changes dramatically. On the same 80^2 mesh, one can see in Fig. 1.2 that the second order finite difference TVD scheme has a much worse resolution than the fifth order finite difference WENO scheme. Clearly the result of the second order scheme with this mesh for this long time is completely unacceptable. This time, even if one increases the number of mesh points to 320^2 for the second order scheme (which makes the CPU time for such a run magnitudes more than that of a fifth order WENO scheme on a 80^2 mesh), it still does not provide a satisfactory resolution, Fig. 1.3, right. A more refined mesh would not be practical for three dimensional simulations. Clearly, in this situation the second order scheme is inadequate to provide a satisfactory resolution within the limit of today's computer.

There are many high order methods being used in CFD. In this paper we only discuss

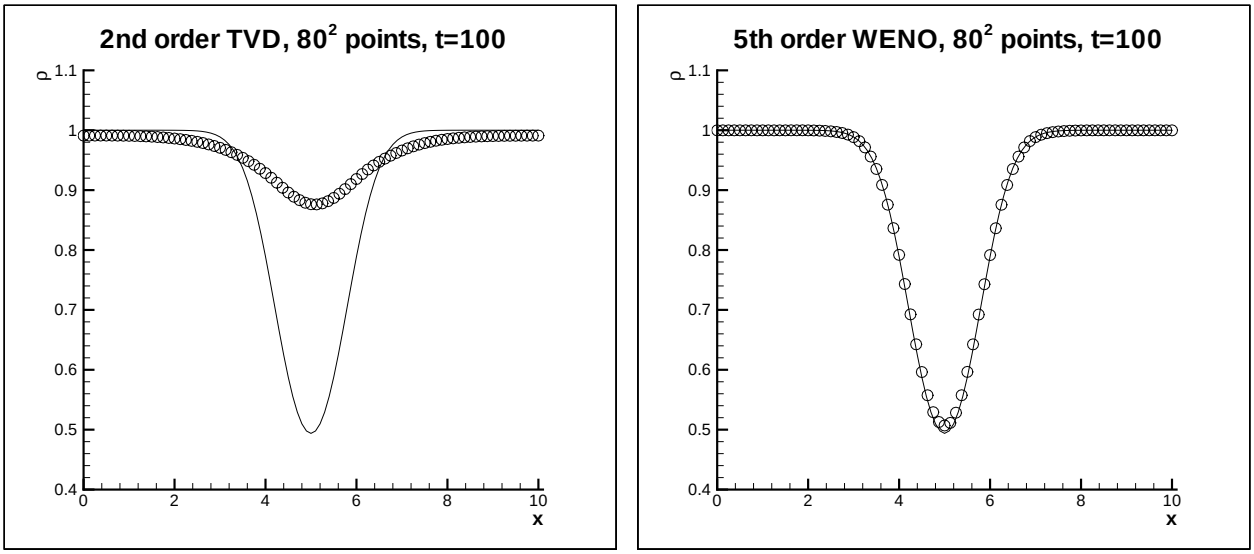

Figure 1.2: Vortex evolution. Cut at $x = 5$. Density ρ. 80^2 uniform mesh. $t = 100$ (after 10 time periods). Solid: exact solution; circles: computed solution. Left: second order TVD scheme; right: fifth order WENO scheme.

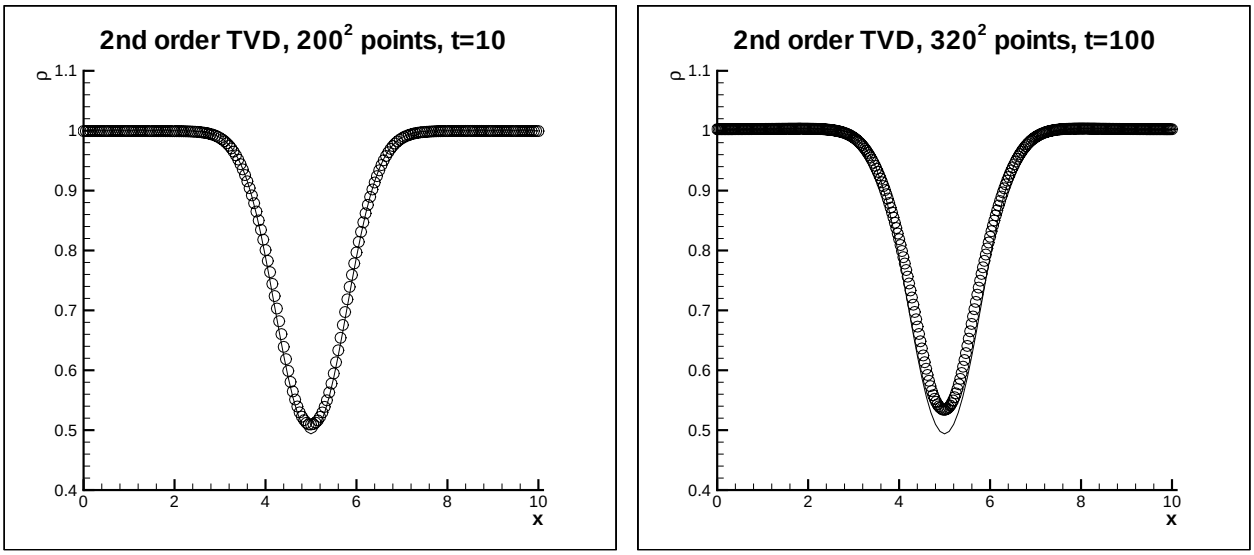

Figure 1.3: Vortex evolution. Cut at $x = 5$. Density ρ. Second order TVD scheme. Solid: exact solution; circles: computed solution. Left: 200^2 uniform mesh, $t = 10$ (after one time period); right: 320^2 uniform mesh, $t = 100$ (after 10 time periods).

three types of them:

1. The weighted essentially non-oscillatory (WENO) finite difference methods;

2. The WENO finite volume methods;

3. The discontinuous Galerkin (DG) finite element methods.

These are methods suitable for solving hyperbolic conservation laws, such as the compressible Euler equations (1.1), or convection dominated convection diffusion problems, such as the compressible Navier-Stokes equations with high Reynolds numbers. For such problems shocks and other discontinuities or high gradient regions exist in the solutions, making it difficult to design stable and high order numerical methods.

Let us first give some historical remarks about these methods.

WENO schemes are designed based on the successful essentially non-oscillatory (ENO) schemes in [19, 43, 44]. The first WENO scheme is constructed in [31] for a third order finite volume version in one space dimension. In [23], third and fifth order finite difference WENO schemes in multi space dimensions are constructed, with a general framework for the design of the smoothness indicators and nonlinear weights. Later, second, third and fourth order finite volume WENO schemes for 2D general triangulation have been developed in [14] and [20]. Very high order finite difference WENO schemes (for orders between 7 and 11) have been developed in [2]. Central WENO schemes have been developed in [25], [26] and [27].

Both ENO and WENO use the idea of adaptive stencils in the reconstruction procedure based on the local smoothness of the numerical solution to automatically achieve high order accuracy and non-oscillatory property near discontinuities. ENO uses just one (optimal in some sense) out of many candidate stencils when doing the reconstruction; while WENO uses a convex combination of all the candidate stencils, each being assigned a nonlinear weight which depends on the local smoothness of the numerical solution based on that stencil. WENO improves upon ENO in robustness, better smoothness of fluxes, better steady state

convergence, better provable convergence properties, and more efficiency. For more details of ENO and WENO schemes, we refer to the lecture notes [41, 42].

WENO schemes have been widely used in applications. Some of the examples include dynamical response of a stellar atmosphere to pressure perturbations [13]; shock vortex interactions and other gas dynamics problems [17], [18]; incompressible flow problems [47]; Hamilton-Jacobi equations [21]; magneto-hydrodynamics [24]; underwater blast-wave focusing [28]; the composite schemes and shallow water equations [29], [30], real gas computations [32], wave propagation using Fey's method of transport [33]; etc.

Discontinuous Galerkin (DG) methods are a class of finite element methods using completely discontinuous basis functions, which are usually chosen as piecewise polynomials. Since the basis functions can be completely discontinuous, these methods have the flexibility which is not shared by typical finite element methods, such as the allowance of arbitrary triangulation with hanging nodes, complete freedom in changing the polynomial degrees in each element independent of that in the neighbors (p adaptivity), and extremely local data structure (elements only communicate with immediate neighbors regardless of the order of accuracy of the scheme) and the resulting embarrassingly high parallel efficiency (usually more than 99% for a fixed mesh, and more than 80% for a dynamic load balancing with adaptive meshes which change often during time evolution), see, e.g. [4]. A very good example to illustrate the capability of the discontinuous Galerkin method in h-p adaptivity, efficiency in parallel dynamic load balancing, and excellent resolution properties is the recent successful simulation of the Rayleigh-Taylor flow instabilities in [36].

The first discontinuous Galerkin method was introduced in 1973 by Reed and Hill [35], in the framework of neutron transport, i.e. a time independent linear hyperbolic equation. A major development of the DG method is carried out by Cockburn et al. in a series of papers [6, 7, 8, 9], in which they have established a framework to easily solve *nonlinear* time dependent problems, such as the Euler equations (1.1), using explicit, nonlinearly stable high order Runge-Kutta time discretizations [43] (see section 2) and DG discretization in space

with exact or approximate Riemann solvers as interface fluxes and total variation bounded (TVB) nonlinear limiters to achieve non-oscillatory properties for strong shocks.

The DG method has found rapid applications in such diverse areas as aeroacoustics, electro-magnetism, gas dynamics, granular flows, magneto-hydrodynamics, meteorology, modeling of shallow water, oceanography, oil recovery simulation, semiconductor device simulation, transport of contaminant in porous media, turbomachinery, turbulent flows, viscoelastic flows and weather forecasting, among many others. For more details, we refer to the survey paper [12], and other papers in that Springer volume, which contains the conference proceedings of the First International Symposium on Discontinuous Galerkin Methods held at Newport, Rhode Island in 1999. The extensive review paper [11] is also a good reference for many details.

This paper is written from a practical user's point of view. We will not emphasize the discussion of theoretical properties of the schemes. Rather, we will indicate the practical aspects in the implementation of the algorithms, their applicability in different situations, and their relative advantages, and present a few selected numerical examples to demonstrate their performance on illustrative model CFD problems.

2 Time discretizations

Before discussing the spatial discretizations, let us first discuss the time discretization. For all three types of spatial discretizations discussed in this paper, we shall use the same time discretization, namely a class of high order nonlinearly stable Runge-Kutta time discretizations. A distinctive feature of this class of time discretizations is that they are convex combinations of first order forward Euler steps, hence they maintain strong stability properties in any semi-norm (total variation norm, maximum norm, entropy condition, etc.) of the forward Euler step. Thus one only needs to prove nonlinear stability for the first order forward Euler step, which is relatively easy in many situations (e.g. TVD schemes), and one automatically obtains the same strong stability property for the higher order time discretizations in this

class. These methods were first developed in [43] and [40], and later generalized in [15] and [16]. The most popular scheme in this class is the following third order Runge-Kutta method for solving

$$u_t = L(u,t)$$

where $L(u,t)$ is a spatial discretization operator (it does not need to be, and often is not, linear!):

$$\begin{aligned} u^{(1)} &= u^n + \Delta t L(u^n, t^n) \\ u^{(2)} &= \frac{3}{4}u^n + \frac{1}{4}u^{(1)} + \frac{1}{4}\Delta t L(u^{(1)}, t^n + \Delta t) \\ u^{n+1} &= \frac{1}{3}u^n + \frac{2}{3}u^{(2)} + \frac{2}{3}\Delta t L(u^{(2)}, t^n + \frac{1}{2}\Delta t). \end{aligned}$$

All the numerical examples presented in this paper are obtained with this Runge-Kutta time discretization.

3 Finite difference WENO schemes

A conservative finite difference spatial discretization to a conservation law such as (1.1) approximates the derivative $f(u)_x$ by a conservative difference

$$f(u)_x|_{x=x_j} \approx \frac{1}{\Delta x}\left(\hat{f}_{j+1/2} - \hat{f}_{j-1/2}\right)$$

where $\hat{f}_{j+1/2}$ is the numerical flux, which typically is a Lipschitz continuous function of several neighboring values u_i. $g(u)_y$ is approximated in the same way. Hence finite difference methods have the same format for one and several space dimensions, which is a big advantage. For the simplest case of a scalar equation (1.1) and if $f'(u) \geq 0$, the fifth order finite difference WENO scheme has the flux given by

$$\hat{f}_{j+1/2} = w_1 \hat{f}^{(1)}_{j+1/2} + w_2 \hat{f}^{(2)}_{j+1/2} + w_3 \hat{f}^{(3)}_{j+1/2}$$

where $\hat{f}^{(i)}_{j+1/2}$ are three third order fluxes on three different stencils given by

$$\begin{aligned}
\hat{f}^{(1)}_{j+1/2} &= \frac{1}{3}f(u_{j-2}) - \frac{7}{6}f(u_{j-1}) + \frac{11}{6}f(u_j), \\
\hat{f}^{(2)}_{j+1/2} &= -\frac{1}{6}f(u_{j-1}) + \frac{5}{6}f(u_j) + \frac{1}{3}f(u_{j+1}), \\
\hat{f}^{(3)}_{j+1/2} &= \frac{1}{3}f(u_j) + \frac{5}{6}f(u_{j+1}) - \frac{1}{6}f(u_{j+2}),
\end{aligned}$$

and the nonlinear weights w_i are given by

$$w_i = \frac{\tilde{w}_i}{\sum_{k=1}^{3} \tilde{w}_k}, \qquad \tilde{w}_k = \frac{\gamma_k}{(\varepsilon + \beta_k)^2},$$

with the linear weights γ_k given by

$$\gamma_1 = \frac{1}{10}, \qquad \gamma_2 = \frac{3}{5}, \qquad \gamma_3 = \frac{3}{10},$$

and the smoothness indicators β_k given by

$$\begin{aligned}
\beta_1 &= \frac{13}{12}\left(f(u_{j-2}) - 2f(u_{j-1}) + f(u_j)\right)^2 + \frac{1}{4}\left(f(u_{j-2}) - 4f(u_{j-1}) + 3f(u_j)\right)^2 \\
\beta_2 &= \frac{13}{12}\left(f(u_{j-1}) - 2f(u_j) + f(u_{j+1})\right)^2 + \frac{1}{4}\left(f(u_{j-1}) - f(u_{j+1})\right)^2 \\
\beta_3 &= \frac{13}{12}\left(f(u_j) - 2f(u_{j+1}) + f(u_{j+2})\right)^2 + \frac{1}{4}\left(3f(u_j) - 4f(u_{j+1}) + f(u_{j+2})\right)^2 .
\end{aligned}$$

Finally, ε is a parameter to avoid the denominator to become 0 and is usually taken as $\varepsilon = 10^{-6}$ in the computation.

This finishes the description of the fifth order finite difference WENO scheme [23] in the simplest case. As we can see, the algorithm is actually quite simple and there is no tunable parameters in the scheme.

We summarize the properties of this WENO finite difference scheme. For details of proofs and numerical verifications, see [23] and [41, 42].

1. The scheme is proven to be uniformly fifth order accurate including at smooth extrema, and this is verified numerically.

2. Near discontinuities the scheme behaves very similarly to an ENO scheme [19, 43, 44], namely the solution has a sharp and non-oscillatory discontinuity transition.

3. The numerical flux has the same smoothness dependency on its arguments as that of the physical flux $f(u)$. This helps in a convergence analysis for smooth solutions and in steady state convergence.

4. The approximation is self similar. That is, when fully discrete with Runge-Kutta methods in section 2, the scheme is invariant when the spatial and time variables are scaled by the same factor.

We then indicate how the scheme is generalized in a more complex situation:

1. For scalar equations without the property $f'(u) \geq 0$, one could use a flux splitting

$$f(u) = f^+(u) + f^-(u), \qquad \frac{df^+(u)}{du} \geq 0, \ \ \frac{df^-(u)}{du} \leq 0,$$

and apply the procedure above to $f^+(u)$, and a mirror image (with respect to $j+1/2$) procedure to $f^-(u)$. The only requirement for the splitting is that $f^{\pm}(u)$ should be as smooth functions of u as $f(u)$ is and as the order of the scheme requires (e.g. if the scheme is fifth order, $f(u)$ and $f^{\pm}(u)$ should all have five continuous derivatives with respect to u). In most applications the simple Lax-Friedrichs flux splitting

$$f^{\pm}(u) = \frac{1}{2}(f(u) \pm \alpha u), \qquad \alpha = max_u |f'(u)|$$

where the maximum is taken over the relevant range of u, is a good choice.

2. For systems of hyperbolic conservation laws, the nonlinear part of the WENO procedure (i.e. the determination of the smoothness indicators β_k and hence the nonlinear weights w_i) should be carried out in local characteristic fields. Thus one would first find an average $u_{j+1/2}$ of u_j and u_{j+1} (e.g. the Roe average [37] which exists for many physical systems), and compute the left and right eigenvectors of the Jacobian $f'(u_{j+1/2})$ and put them into the rows of $R^{-1}_{j+1/2}$ and the columns of $R_{j+1/2}$, respectively, such that $R^{-1}_{j+1/2} f'(u_{j+1/2}) R_{j+1/2} = \Lambda_{j+1/2}$ where $\Lambda_{j+1/2}$ is a diagonal matrix containing the real eigenvalues of $f'(u_{j+1/2})$. One then transforms all the quantities needed for evaluating

the numerical flux $\hat{f}_{j+1/2}$ to the local characteristic fields by left multiplying them with $R^{-1}_{j+1/2}$, and then computes the numerical fluxes by the scalar procedure in each characteristic field. Finally, the flux in the original physical space is obtained by left multiplying the numerical flux obtained in the local characteristic fields with $R_{j+1/2}$.

3. If one has a non-uniform but smooth mesh, for example $x = x(\xi)$ where ξ_j is uniform and $x(\xi)$ has at least five continuous derivatives for the fifth order method, then one could use the chain rule $f(u)_x = f(u)_\xi / x'(\xi)$ and simply use the procedure above for uniform meshes to approximate $f(u)_\xi$. The metric derivative $x'(\xi)$ should be either obtained through an analytical formula (if the transformation $x = x(\xi)$ is explicitly given) or by a finite difference approximation which is at least fifth order accurate, for example again by a WENO approximation. Using this, one could use finite difference WENO schemes on smooth curvilinear coordinates in any space dimension.

4. WENO finite difference schemes are available for all odd orders, see [23] and [2] for the formulas of the third order and seventh through eleventh order WENO schemes.

We present two numerical examples to illustrate the capability of the finite difference WENO schemes. Both are obtained with the fifth order WENO schemes.

The first example is the double Mach reflection problem, originally given in [45] and later used often in the literature as a benchmark. The computational domain is $[0, 4] \times [0, 1]$, although typically only the results in $[0, 3] \times [0, 1]$ are shown in the figures. The reflecting wall lies at the bottom, starting from $x = \frac{1}{6}$. Initially a right-moving Mach 10 shock is positioned at $x = \frac{1}{6}, y = 0$ and makes a 60° angle with the x axis. For the bottom boundary, the exact post-shock condition is imposed for the part from $x = 0$ to $x = \frac{1}{6}$ and a reflective boundary condition is used for the rest. At the top boundary, the flow values are set to describe the exact motion of a Mach 10 shock. The computation is carried out to $t = 0.2$. At a very refined resolution, the slip line induced instability and roll-up can be observed, see, e.g. the adaptive mesh simulation in [3]. The capability of a numerical method to simulate these

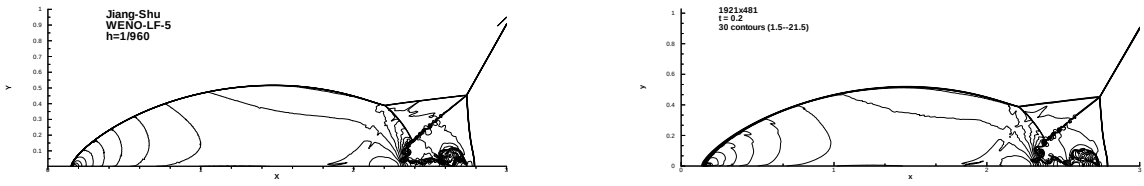

Figure 3.1: Density contours, double Mach reflection, fifth order finite difference WENO scheme. Left: uniform mesh with $\Delta x = \Delta y = \frac{1}{960}$; Right: non-uniform moving mesh with 1/4 as many 2D mesh points (480 points in y).

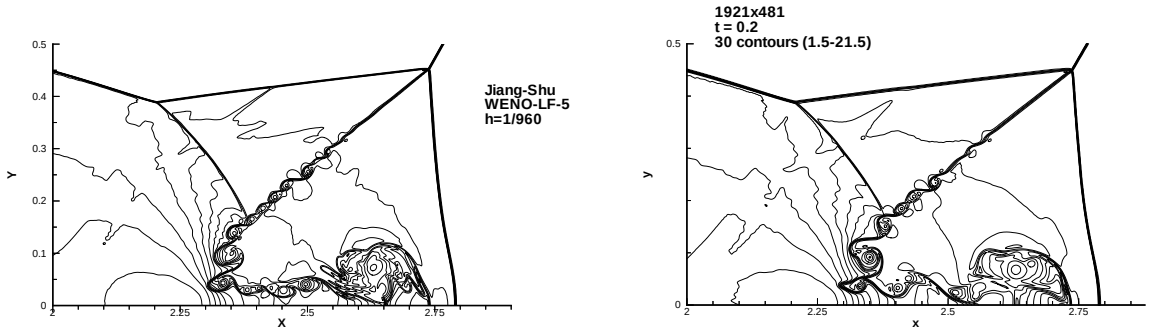

Figure 3.2: A "zoomed in" version of the density contours, double Mach reflection, fifth order finite difference WENO scheme. Left: uniform mesh with $\Delta x = \Delta y = \frac{1}{960}$; Right: non-uniform moving mesh with 1/4 as many 2D mesh points (480 points in y).

roll-ups is an indication of its small numerical viscosity and high resolution. In Fig. 3.1, left, we give the density contours of the simulation result with the fifth order WENO scheme on a fixed, uniform mesh with $\Delta x = \Delta y = \frac{1}{960}$. In Fig. 3.1, right, we give the density contours of the simulation result with the fifth order WENO scheme on a non-uniform and moving mesh, which is smooth and concentrates its points near the shock and the region under the double Mach stem, with only half the number of points in each direction (480 points in y). The mesh movements were determined by a given smooth transformation which follows the structure of the solution. Fig. 3.2 gives a "zoomed in" picture. We can clearly see that the resolutions are comparable while the moving non-uniform mesh version uses only 1/4 as many 2D mesh points as the uniform one, hence saving a lot of computational effort.

The second example is the problem of a supersonic flow past a cylinder [23]. In the physical space, a cylinder of unit radius is positioned at the origin on the x-y plane. The

computational domain is chosen to be $[0,1] \times [0,1]$ on the ξ-η plane. The mapping between the computational domain and the physical domain is:

$$x = (R_x - (R_x - 1)\xi)\cos(\theta(2\eta - 1)), \qquad y = (R_y - (R_y - 1)\xi)\sin(\theta(2\eta - 1)),$$

where $R_x = 3, R_y = 6$ and $\theta = \frac{5\pi}{12}$. Fifth order finite difference WENO and a uniform mesh of 60×80 points in the computational domain are used. The problem is initialized by a Mach 3 shock moving towards the cylinder from the left. Reflective boundary condition is imposed at the surface of the cylinder, i.e. at $\xi = 1$, inflow boundary condition is applied at $\xi = 0$ and outflow boundary condition is applied at $\eta = 0, 1$. We present an illustration of the mesh in the physical space (drawn every other grid line), and the pressure contour, in Fig. 3.3. We can clearly see that the finite difference WENO scheme can handle such curvilinear meshes very well.

In summary, we can say the following about finite difference WENO schemes:

1. They can only be used for regular geometry that can be covered either by uniform or smooth curvilinear meshes. The smoothness of the mesh must be comparable with the order of accuracy of the scheme in order to obtain a truly high order result.

2. If the computational problem allows for such meshes, then the finite difference WENO schemes are good choices as they are easy to code and fast to compute, especially for multi dimensional problems. Usually the fifth order WENO scheme is the best choice, unless the nature of the problem asks for higher orders of resolution.

3. The finite difference WENO schemes can also be used in an adaptive mesh environment, provided that a smooth (in space and time) mesh can be generated. To generate such meshes is not easy, especially for higher order schemes where the requirement for the smoothness of the meshes is stronger.

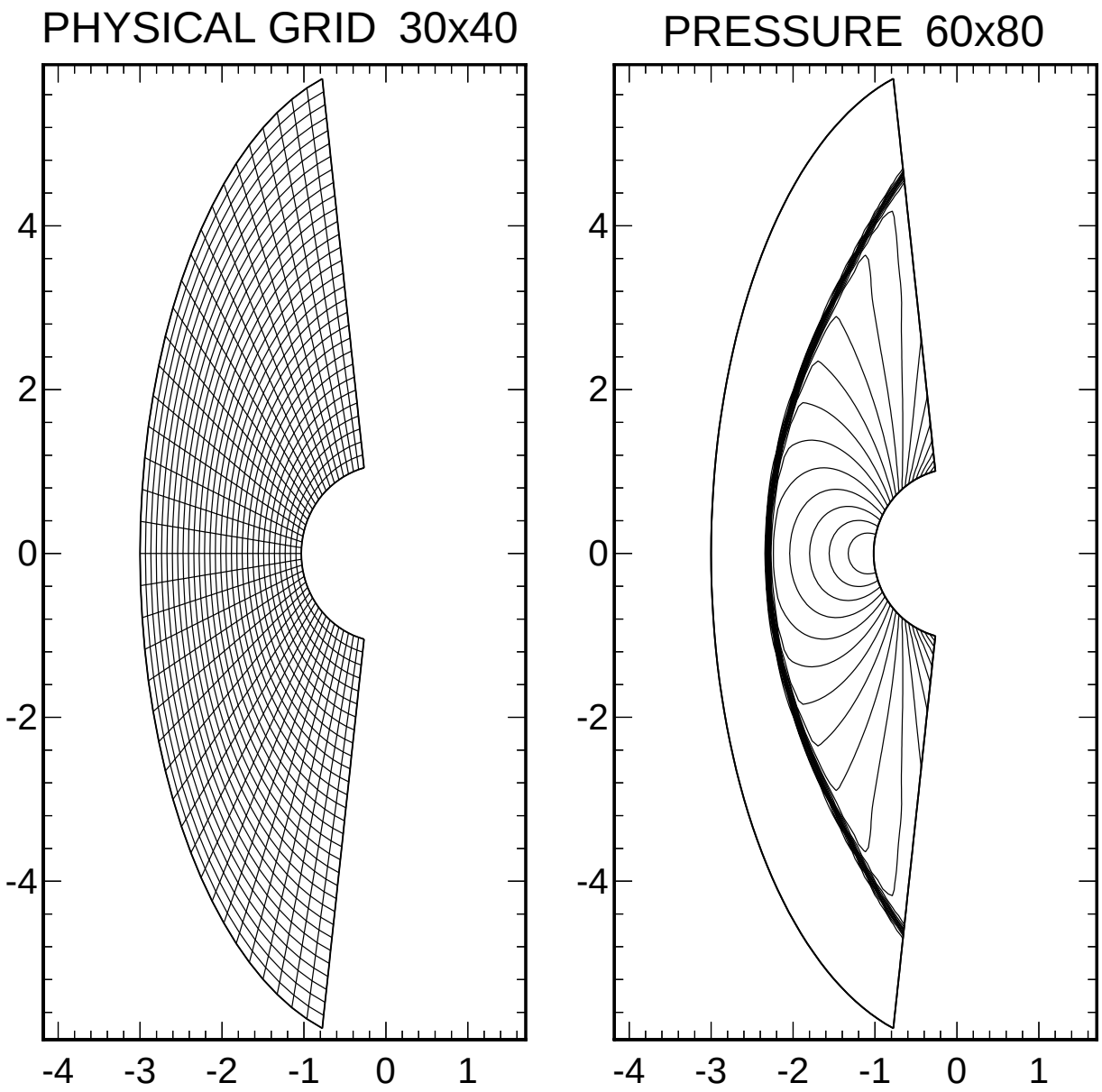

Figure 3.3: Flow past a cylinder. Left: physical grid drawn on every other grid line; right: pressure contours with 20 contour lines.

4 Finite volume WENO schemes

A finite volume scheme for a conservation law such as (1.1) approximates an integral version of it. Thus, the computational domain is partitioned into a collection of cells $\triangle_i$, which in 2D could be rectangles, triangles, etc., and the cell averages of the solution u

$$\bar{u}_i(t) \equiv \frac{1}{|\triangle_i|} \int_{\triangle_i} u(x,y,t)dxdy$$

are the numerically approximated quantities. If $\triangle_j$ is a control volume, the semi-discrete finite volume scheme of equation (1.1) is:

$$\frac{d}{dt}\bar{u}_j(t) + \frac{1}{|\triangle_j|} \int_{\partial\triangle_j} F \cdot n \, ds \; = \; 0 \tag{4.1}$$

where $F = (f, g)$, and n is the outward unit normal of the cell boundary $\partial\triangle_j$. The line integral in (4.1) is typically discretized by a Gaussian quadrature of sufficiently high order of accuracy,

$$\int_{\partial\triangle_j} F \cdot n \, ds \; \approx \; |\partial\triangle_j| \sum_{k=1}^{q} \omega_k F(u(G_k,t)) \cdot n$$

and $F(u(G_k,t)) \cdot n$ is replaced by a numerical flux (approximate or exact Riemann solvers). For example, one could use the simple Lax-Friedrichs flux, which is given by

$$F(u(G_k,t)) \cdot n \; \approx \; \frac{1}{2}\left[\left(F(u^-(G_k,t)) + F(u^+(G_k,t))\right) \cdot n - \alpha\left(u^+(G_k,t) - u^-(G_k,t)\right)\right]$$

where α is taken as an upper bound for the eigenvalues of the Jacobian in the n direction, and u^- and u^+ are the values of u inside the cell $\triangle_j$ and outside the cell $\triangle_j$ (inside the neighboring cell) at the Gaussian point G_k.

Clearly, the success of the finite volume scheme depends crucially on a good "reconstruction" procedure, which is the procedure to obtain high order and non-oscillatory approximations to the solution u at the Gaussian points along the cell boundary, $u^{\pm}(G_k,t)$, from the neighboring cell averages. Usually, this reconstruction problem is handled in the following way: given a stencil of $R = \frac{(r+1)(r+2)}{2}$ cells, find a polynomial of degree r, whose cell average in each cell within the stencil agrees with the given cell average of u in that cell. This

gives a linear system of R equations and R unknowns (the coefficients of the polynomial when expanded in a certain basis), and, if it has a unique solution, the polynomial can be evaluated at the Gaussian point to get the approximation to $u^{\pm}(G_k, t)$. In practice, there are a lot of complications in this procedure, as not all stencils result in a solvable or well conditioned linear system. One would often resort to a least square procedure with more than the necessary number of cells in the stencil to solve this problem, see, e.g. [20]. If the cells are rectangles rather than triangles, then a tensor product polynomial and a tensor product stencil would be much easier to work with [38].

A typical WENO finite volume scheme is constructed as follows:

1. We identify several stencils $\mathcal{S}_i$, $i = 1, ..., q$, such that the control volume $\triangle_j$ belongs to each stencil. We denote by $\mathcal{T} = \bigcup_{i=1}^{q} \mathcal{S}_i$ the larger stencil which contains all the cells from the q stencils.

2. We obtain a (relatively) lower order reconstruction polynomial, denoted by $p_i(x)$, associated with each of the stencils $\mathcal{S}_i$, for $i = 1, ..., q$. We also obtain a (relatively) higher order reconstruction polynomial, denoted by $P(x)$, associated with the larger stencil $\mathcal{T}$.

3. We find the combination coefficients, also called linear weights, denoted by γ_1, ... , γ_q, such that for a Gaussian point G_k on the cell boundary,

$$P(G_k) = \sum_{i=1}^{q} \gamma_i p_i(G_k)$$

for all possible given cell averages in the stencil. These linear weights depend on the mesh geometry, the point G_k, and the specific reconstruction requirements, but *not* on the given cell averages in the stencil.

4. We compute the smoothness indicator, denoted by β_i, for each stencil $\mathcal{S}_i$, which measures how smooth the function $p_i(x)$ is in the target cell $\triangle_j$. The smaller this smoothness indicator β_i, the smoother the function $p_i(x)$ is in the target cell. These smooth-

ness indicators are obtained with the same integral formulas as in the finite difference WENO schemes. The details can be found in [20] and [38].

5. We compute the nonlinear weights based on the smoothness indicators:

$$w_i = \frac{\tilde{w}_i}{\sum_k \tilde{w}_k}, \qquad \tilde{w}_k = \frac{\gamma_k}{(\varepsilon + \beta_k)^2}$$

where γ_k are the linear weights determined in step 3 above, and ε is again a small number to avoid the denominator to become 0 and is usually taken as $\varepsilon = 10^{-6}$ in the computations. The final WENO reconstruction is then given by

$$u^-(G_k) = \sum_{i=1}^{q} w_i p_i(G_k).$$

We summarize the properties of this WENO finite volume scheme. For more details, see [20] and [38].

1. For 2D triangulation with arbitrary triangles, third and fourth order finite volume WENO schemes are available, [20], [38]. The third order scheme is quite robust. The fourth order scheme, however, seems to have more restrictive requirements on the triangulation for stability for solving systems of conservation laws.

2. For 2D triangulation with tensor product rectangle meshes, which could be non-uniform and non-smooth, the fifth order WENO scheme in [38] is quite robust and gives very good numerical results.

We will again use the double Mach reflection problem to illustrate the behavior of the finite volume WENO schemes. To save space we will show only the results obtained with the fifth order finite volume WENO scheme on a tensor product mesh, with a uniform mesh of $\Delta x = \Delta y = \frac{1}{480}$ [38], in Fig. 4.1. Results obtained with the third and fourth order WENO schemes on triangular meshes can be found in [20].

In summary, we can say the following about finite volume WENO schemes:

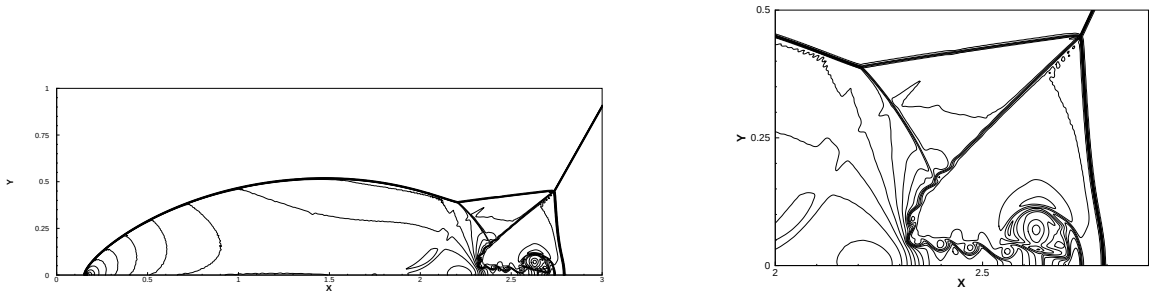

Figure 4.1: Double Mach reflection, fifth order finite volume WENO scheme, uniform mesh with $\Delta x = \Delta y = \frac{1}{480}$. Left: density contours; Right: a "zoomed in" version of the density contours.

1. They can be used for arbitrary triangulation. However they are much more complex to code and much more expensive in CPU cost than finite difference WENO schemes of the same order of accuracy. This is because they have to rely on multidimensional reconstructions (polynomials of 2 or 3 variables in 2D or 3D), and the flux integrals on the cell boundaries must be performed by multi point Gaussian quadratures. As a rule of thumb, a finite volume WENO scheme is at least 4 times more expensive in 2D and 9 times more expensive in 3D, compared with a finite difference WENO scheme on the same mesh and of the same order of accuracy, see, e.g. [5] for such a comparison for ENO schemes.

2. Finite volume WENO schemes on a tensor product mesh are more robust and can be constructed for higher order of accuracy than finite volume WENO schemes on arbitrary triangulation.

3. Finite volume WENO schemes should be used in the situation when it is impossible to apply a smooth curvilinear mesh.

5 Discontinuous Galerkin methods

Similar to a finite volume scheme, a discontinuous Galerkin (DG) method for a conservation law such as (1.1) also approximates an integral version of it. The computational domain is

again partitioned into a collection of cells $\triangle_i$, which in 2D could be rectangles, triangles, etc., and the numerical solution is a polynomial of degree r in each cell $\triangle_i$. The degree r could change with the cell, and there is no continuity requirement of the two polynomials along an interface of two cells. Thus, instead of only one degree of freedom per cell in a finite volume scheme, namely the cell average of the solution, there are $R = \frac{(r+1)(r+2)}{2}$ degrees of freedom per cell for a DG method using piecewise r-th degree polynomials in 2D. These R degrees of freedom are chosen as the coefficients of the polynomial when expanded in a local basis. One could use a locally orthogonal basis to simplify the computation, but this is not essential.

The DG method is obtained by multiplying (1.1) by a test function $v(x, y)$ (which is also a polynomial of degree r in the cell), integrating over the cell $\triangle_j$, and integrating by parts:

$$\frac{d}{dt}\int_{\triangle_j} u(x,y,t)v(x,y)dxdy - \int_{\triangle_j} F(u)\cdot\nabla v\, dxdy + \int_{\partial\triangle_j} F(u)\cdot n\, v\, ds \;=\; 0$$

where the notation and the treatment of the line integral are the same as in the finite volume scheme (4.1). The extra volume integral term $\int_{\triangle_j} F(u)\cdot\nabla v\, dxdy$ can be computed either by a numerical quadrature or by a quadrature free implementation [1] for special systems such as the Euler equations (1.1). Notice that if a locally orthogonal basis is chosen, the time derivative term $\frac{d}{dt}\int_{\triangle_j} u(x,y,t)v(x,y)dxdy$ would be explicit and there is no mass matrix to invert. However, even if the local basis is not orthogonal, one still only needs to invert a small $R \times R$ local mass matrix (by hand) and there is never a global mass matrix to invert as in a typical finite element method.

When applied to problems with smooth solutions, the DG method as briefly described above can already be used as is. For problems containing discontinuous solutions, however, a nonlinear total variation bounded (TVB) limiter might be needed. For details, see [39, 6, 8, 9].

We summarize the properties of the DG method here. For more details, see [11].

1. The DG method has the best provable stability property among all three methods discussed in this paper. One can prove a cell entropy inequality for the square entropy

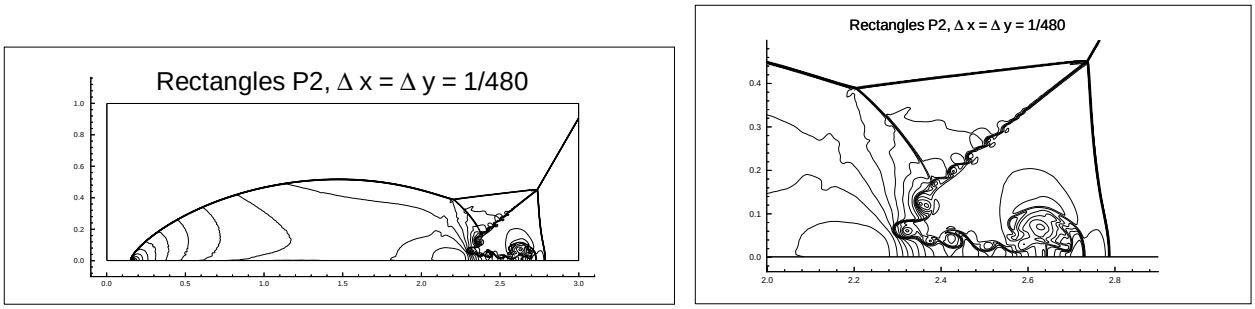

Figure 5.1: Double Mach reflection, third order (P^2 polynomials) discontinuous Galerkin method, rectangular uniform mesh with $\Delta x = \Delta y = \frac{1}{480}$. Left: density contours; Right: a "zoomed in" version of the density contours.

[22], which implies L^2 stability for the full nonlinear case with possible discontinuous solutions, and any converged solution is an entropy solution for a convex scalar conservation law. This cell entropy inequality holds for all scalar nonlinear conservation laws, all orders of accuracy of the scheme, all space dimensions, arbitrary triangulation, and without the need to use the nonlinear limiters.

2. The DG method can also be used on problems with second derivatives (diffusion terms such as those from the Navier-Stokes equations), [10], [34]. It can even be used on problems with third derivative terms [46]. Theoretical results about stability and rate of convergence are very similar to those for the first derivative PDEs. Unlike the traditional mixed method, such local discontinuous Galerkin methods for higher derivatives are truly local (the auxiliary variables introduced for the derivatives can be eliminated locally) and share with the discontinuous Galerkin method all the flexibility and advantages such as a tolerance of arbitrary triangulation with hanging nodes, parallel efficiency, easiness in *h-p* adaptivity, etc.

We will again use the double Mach reflection problem to illustrate the behavior of the DG methods. We present the result of the third order method (piecewise quadratic polynomials) on a rectangular mesh with $\Delta x = \Delta y = \frac{1}{480}$ [9], in Fig. 5.1.

In summary, we can say the following about the discontinuous Galerkin methods:

1. They can be used for arbitrary triangulation, including those with hanging nodes. Moreover, the degree of the polynomial, hence the order of accuracy, in each cell can be independently decided. Thus the method is ideally suited for *h-p* (mesh size and order of accuracy) refinements and adaptivity.

2. The methods have excellent parallel efficiency. Even with space time adaptivity and load balancing the parallel efficiency can still be over 80%.

3. They should be the methods of choice if geometry is complicated or if adaptivity is important, especially for problems with smooth solutions.

4. For problems containing strong shocks, the nonlinear limiters are still less robust than the advanced WENO philosophy. There is a parameter (the TVB constant) for the user to tune for each problem. For rectangular meshes the limiters work better than for triangular ones. Other limiters are still being investigated in the literature.

6 Concluding remarks

We have discussed three classes of typical high order numerical methods used in CFD, especially for problems containing both shocks or high gradient regions and complex smooth region structures. These are finite difference WENO schemes, finite volume WENO schemes and discontinuous Galerkin methods. All three methods use the same nonlinearly stable high order Runge-Kutta time discretizations [43], hence their difference is only in spatial discretizations. Finite difference WENO schemes have the advantage of simplicity and lower CPU cost, especially for multi dimensional problems, but they can only be applied on smooth structured curvilinear meshes. If a computational problem allows the usage of such meshes, finite difference WENO schemes are good choices. In this class the one used most often is the fifth order WENO scheme in [23]. Finite volume WENO schemes are more expensive than their finite difference counter parts. However, they do have the advantage of allowing arbitrary triangulation, at least in principle. For two dimensional triangulation with arbitrary

triangles, WENO finite volume schemes of third and fourth order accuracy are available [20], [38]. The third order version is quite robust, however the fourth order version seems to have more restrictive requirements on the type of triangulation for stability. Higher order versions and three dimensional cases are still under development. For structured meshes, finite volume WENO schemes of fifth order accuracy [38] are very robust and allow for arbitrary, non-smooth mesh sizes, hence they can be used in more general situations than the finite difference WENO schemes. Finally, the discontinuous Galerkin method is the most flexible in terms of arbitrary triangulation and boundary conditions. It is ideally suited for problems with smooth solutions. For problems containing shocks, the total variation bounded limiter [39, 6, 8, 9] works quite well for rectangular meshes, and reasonably well for arbitrary triangulation. However they are still less robust than WENO schemes as they contain a tuning parameter. An active research direction now is the search for a more robust and high order preserving limiter for general triangulation.

References

[1] H. Atkins and C.-W. Shu, *Quadrature-free implementation of the discontinuous Galerkin method for hyperbolic equations*, AIAA J., v36 (1998), pp.775-782.

[2] D. Balsara and C.-W. Shu, *Monotonicity preserving weighted essentially non-oscillatory schemes with increasingly high order of accuracy*, J. Comput. Phys., v160 (2000), pp.405-452.

[3] M. Berger and A. Colella, *Local adaptive mesh refinement for shock hydrodynamics*, J. Comput. Phys., v82 (1989), pp.64-84.

[4] R. Biswas, K. D. Devine and J. Flaherty, *Parallel, adaptive finite element methods for conservation laws*, Appl. Numer. Math., v14 (1994), pp.255-283.

[5] J. Casper, C.-W. Shu and H.L. Atkins, *Comparison of two formulations for high-order accurate essentially nonoscillatory schemes*, AIAA J., v32 (1994), pp.1970-1977.

[6] B. Cockburn and C.-W. Shu, *TVB Runge-Kutta local projection discontinuous Galerkin finite element method for scalar conservation laws II: general framework*, Math. Comp., v52 (1989), pp.411-435.

[7] B. Cockburn, S.-Y. Lin and C.-W. Shu, *TVB Runge-Kutta local projection discontinuous Galerkin finite element method for conservation laws III: one dimensional systems*, J. Comput. Phys., v84 (1989), pp.90-113.

[8] B. Cockburn, S. Hou, and C.-W. Shu, *TVB Runge-Kutta local projection discontinuous Galerkin finite element method for conservation laws IV: the multidimensional case*, Math. Comp., v54 (1990), pp.545-581.

[9] B. Cockburn and C.-W. Shu, *TVB Runge-Kutta local projection discontinuous Galerkin finite element method for scalar conservation laws V: multidimensional systems*, J. Comput. Phys., v141 (1998), pp.199-224.

[10] B. Cockburn and C.-W. Shu, *The local discontinuous Galerkin method for time-dependent convection diffusion systems*, SIAM J. Numer. Anal., v35 (1998), pp.2440-2463.

[11] B. Cockburn and C.-W. Shu, *Runge-Kutta Discontinuous Galerkin methods for convection-dominated problems*, preprint.

[12] B. Cockburn, G. Karniadakis and C.-W. Shu, *The development of discontinuous Galerkin methods*, in *Discontinuous Galerkin Methods: Theory, Computation and Applications*, B. Cockburn, G. Karniadakis and C.-W. Shu, editors, Lecture Notes in Computational Science and Engineering, volume 11, Springer, 2000, Part I: Overview, pp.3-50.

[13] L. Del Zanna, M. Velli and P. Londrillo, *Dynamical response of a stellar atmosphere to pressure perturbations: numerical simulations*, Astron. Astrophys., v330 (1998), pp.L13-L16.

[14] O. Friedrichs, *Weighted essentially non-oscillatory schemes for the interpolation of mean values on unstructured grids*, J. Comput. Phys., v144 (1998), pp.194–212.

[15] S. Gottlieb and C.-W. Shu, *Total variation diminishing Runge-Kutta schemes*, Math. Comp., v67 (1998), pp.73-85.

[16] S. Gottlieb, C.-W. Shu and E. Tadmor, *Strong stability preserving high order time discretization methods*, SIAM Review, to appear.

[17] F. Grasso and S. Pirozzoli, *Shock-wave-vortex interactions: Shock and vortex deformations, and sound production*, Theor. Comp. Fluid Dyn., v13 (2000), pp.421-456.

[18] F. Grasso and S. Pirozzoli, *Shock wave-thermal inhomogeneity interactions: Analysis and numerical simulations of sound generation*, Phys. Fluids, v12 (2000), pp.205-219.

[19] A. Harten, B. Engquist, S. Osher and S. Chakravarthy, *Uniformly high order essentially non-oscillatory schemes, III*, J. Comput. Phys., v71 (1987), pp.231–303.

[20] C. Hu and C.-W. Shu, *Weighted Essentially Non-Oscillatory Schemes on Triangular Meshes*, J. Comput. Phys., v150 (1999), pp.97-127.

[21] G. Jiang and D.-P. Peng, *Weighted ENO schemes for Hamilton-Jacobi equations*, SIAM J. Sci. Comput., v21 (2000), pp.2126-2143.

[22] G. Jiang and C.-W. Shu, *On cell entropy inequality for discontinuous Galerkin methods*, Math. Comp., v62 (1994), pp.531-538.

[23] G. Jiang and C.-W. Shu, *Efficient implementation of weighted ENO schemes*, J. Comput. Phys., v126 (1996), pp.202–228.

[24] G. Jiang and C.-C. Wu, *A high order WENO finite difference scheme for the equations of ideal magnetohydrodynamics*, J. Comput. Phys., v150 (1999), pp.561-594.

[25] D. Levy, G. Puppo and G. Russo, *Central WENO schemes for hyperbolic systems of conservation laws*, Math. Model. Numer. Anal. (M^2AN), v33 (1999), pp.547-571.

[26] D. Levy, G. Puppo and G. Russo, *Compact central WENO schemes for multidimensional conservation laws*, SIAM J. Sci. Comput., v22 (2000), pp.656-672.

[27] D. Levy, G. Puppo and G. Russo, *A third order central WENO scheme for 2D conservation laws*, Appl. Numer. Math. v33 (2000),415–421.

[28] S. Liang and H. Chen, *Numerical simulation of underwater blast-wave focusing using a high-order scheme*, AIAA J., v37 (1999), pp.1010-1013.

[29] R. Liska and B. Wendroff, *Composite schemes for conservation laws*, SIAM J. Numer. Anal., v35 (1998), pp.2250-2271.

[30] R. Liska and B. Wendroff, *Two-dimensional shallow water equations by composite schemes*, Int. J. Numer. Meth. Fl., v30 (1999), pp.461-479.

[31] X.-D. Liu, S. Osher and T. Chan, *Weighted essentially non-oscillatory schemes*, J. Comput. Phys., v115 (1994), pp.200–212.

[32] P. Montarnal and C.-W. Shu, *Real gas computation using an energy relaxation method and high order WENO schemes*, J. Comput. Phys., v148 (1999), pp.59-80.

[33] S. Noelle, *The MoT-ICE: a new high-resolution wave-propagation algorithm for multidimensional systems of conservation laws based on Fey's method of transport*, J. Comput. Phys., v164 (2000), pp.283-334.

[34] J.T. Oden, Ivo Babuška, and C.E. Baumann, *A discontinuous hp finite element method for diffusion problems*, J. Comput. Phys., v146 (1998), pp.491–519.

[35] W. H. Reed and T. R. Hill, *Triangular mesh methods for the neutron transport equation*, Tech. Report LA-UR-73-479, Los Alamos Scientific Laboratory, 1973.

[36] J.-F. Remacle, J. Flaherty and M. Shephard, *An adaptive discontinuous Galerkin technique with an orthogonal basis applied to Rayleigh-Taylor flow instabilities*, submitted to SIAM Review.

[37] P. Roe, *Approximate Riemann solvers, parameter vectors and difference schemes*, J. Comput. Phys., v27 (1978), pp.1-31.

[38] J. Shi, C. Hu and C.-W. Shu, *A technique of treating negative weights in WENO schemes*, submitted to J. Comput. Phys.

[39] C.-W. Shu, *TVB uniformly high-order schemes for conservation laws*, Math. Comp., v49 (1987), pp.105-121.

[40] C.-W. Shu, *Total-Variation-Diminishing time discretizations*, SIAM J. Sci. Stat. Comput., v9 (1988), pp.1073-1084.

[41] C.-W. Shu, *Essentially non-oscillatory and weighted essentially non-oscillatory schemes for hyperbolic conservation laws*, in *Advanced Numerical Approximation of Nonlinear Hyperbolic Equations*, B. Cockburn, C. Johnson, C.-W. Shu and E. Tadmor (Editor: A. Quarteroni), Lecture Notes in Mathematics, volume 1697, Springer, 1998, pp.325-432.

[42] C.-W. Shu, *High order ENO and WENO schemes for computational fluid dynamics*, in *High-Order Methods for Computational Physics*, T.J. Barth and H. Deconinck, editors, Lecture Notes in Computational Science and Engineering, volume 9, Springer, 1999, pp.439-582.

[43] C.-W. Shu and S. Osher, *Efficient implementation of essentially non-oscillatory shock capturing schemes*, J. Comput. Phys., v77 (1988), pp.439-471.

[44] C.-W. Shu and S. Osher, *Efficient implementation of essentially non-oscillatory shock capturing schemes, II*, J. Comput. Phys., v83 (1989), pp.32-78.

[45] P. Woodward and P. Colella, *The numerical simulation of two-dimensional fluid flow with strong shocks*, J. Comput. Phys., v54 (1984) pp.115–173.

[46] J. Yan and C.-W. Shu, *A local discontinuous Galerkin method for KdV-like equations*, in preparation.

[47] J. Yang, S. Yang, Y. Chen and C. Hsu, *Implicit weighted ENO schemes for the three-dimensional incompressible Navier-Stokes equations*, J. Comput. Phys., v146 (1998), pp.464-487.